A Simple Method to Study Gas Phase Reactions

To understand better the impact of gas phase reactions on chemical vapor deposition, a new experimental method has been developed to isolate and study homogeneous reactions separately from heterogeneous reactions. This new system heats reactant gases by rapidly compressing them to temperatures greater than 1,000 K; the walls of the reactor remain constant at 500 K or less. Pressure and volume measurements determine the mean temperature of the gas. Results from a series of test reactions and simple models show that this apparatus and measurement method work well. The apparatus is inexpensive and simple to use, and has advantages over shock tubes and static systems.

P. W. Morrison, Jr., J. A. Reimer
Department of Chemical Engineering
University of California
Berkeley, CA 94720-9989

Introduction

Chemical vapor deposition (CVD) is a method of depositing thin films from a gas. Typically, the precursor is stable at low temperatures but decomposes at higher temperatures. In most reactor designs the precursor flows toward a heated surface where the molecule decomposes to form a thin film. The semiconductor industry routinely deposits thin films this way; for example, CVD of SiH_4 yields crystalline or polycrystalline silicon, and CVD of a binary mixture of AsH_3 and $(CH_3)_3Ga$ forms films of gallium arsenide. This deposition method is a complicated interaction of gas phase chemistry (homogeneous), surface chemistry (heterogeneous), and mass transport. For example, consider the microscopic behavior of the precursor as it moves toward the heated surface. As the local temperature rises, the molecule may decompose before it arrives at the surface. If the precursor must arrive intact for the desired deposition to occur, then the gas phase chemistry hinders film growth. Conversely, gas phase decomposition may be a necessary precondition for growth to occur. To dissect the many facets of this complex overall mechanism requires isolating each of these individual chemical steps. Our particular interest is the gas phase chemistry and its impact on thin film deposition.

To study successfully the gas phase chemistry in CVD requires two steps:

1. Generation of gas phase intermediates from a parent molecule while minimizing side reactions of the parent on a reactor wall
2. Transportation of those intermediates to the walls for deposition

The first step determines the kinetics of the homogeneous decomposition of the precursor. Physical chemists have developed successful techniques to accomplish this: static pyrolysis, shock tube experiments, and laser-driven pyrolysis. Applying these techniques to CVD reactions is straightforward.

The second step of the analysis determines the characteristics of the films deposited from the intermediates. Knowing this relationship among intermediates and film characteristics permits modification of the reactor and precursor to produce better films. In many ways, this step is the most relevant to thin film technologies. Despite the importance of step two, there is very little information available that links intermediates to film characteristics. In general, most reactor designs achieve pure homogeneous chemistry by restricting mass transport rates to reactor surfaces. Consequently, a reactor that has a pure homogeneous chemistry and relatively high mass transfer rates is very rare. A new reactor design is necessary.

Alternative Designs

The simplest design that overcomes this problem is the static pyrolysis chamber (Purnell and Walsh, 1966). The reactor is a chamber with surfaces on which the parent molecule does not react; however, any daughter of the parent does react on the surface to form film. The hot chamber is filled with reactant and is held at a constant temperature for various lengths of time. Varying the surface to volume ratio of the reactor verifies that the homogeneous reaction is rate-limiting. Note that the chemical inertness of a surface depends on its temperature: a surface inert at 200°C may not be inert at 500°C. Because the gas and surfaces have the same temperature, the independent control of gas chemistry and surface inertness is limited. Consequently, to

keep a homogeneous reaction as the rate-limiting step requires relatively low temperatures and pressures, and therefore deposition times last weeks or months.

Increasing the deposition rate requires increasing the homogeneous reaction rate. The most obvious solution is to raise the gas temperature. This must be done without significantly raising the surface temperature (otherwise, the surface reaction rates may become unacceptably high). Laser heating of the gas is one alternative (Bilenchi et al., 1984; Flint et al., 1984). In this kind of reactor, a CO_2 laser beam passes through a mixture of reactant and inert gas; the beam is parallel to the deposition surface. As the reactant absorbs infrared radiation, collisions between the absorber and inert gas thermalize the absorbed energy, and the local gas temperature rises. The gas temperature is calculated using an energy balance over the reaction zone; energy absorbed equals energy lost via conduction. This method works well although the local gas temperature is somewhat ambiguous. Laser heating has two major disadvantages. From a chemical point of view, this method is risky because the precursor may decompose via a multiphoton absorption process rather than via the desired thermal pathway (Deutsch, 1979). In addition, the technique is expensive and not easily scaled because it requires a high laser power.

Compressive heating is another method of raising the temperature of a gas independently of surface temperature. Shock tubes are one of the most common methods of making kinetic measurements of reactions that are plagued with heterogeneous side reactions (White et al., 1985; Newman et al., 1979). Indeed, this method is the experiment of choice for determination of the preexponential factor, activation energy, and order of reaction at high temperatures. In this experiment, a shock wave propagates down a tube and creates a well-defined zone of hot gas behind it. In principle, measuring the shock velocities is sufficient to determine the temperature of the hot zone. Inaccuracies in the velocity measurements (especially at lower shock strengths and temperature) produce scatter in the results. However, using the comparative rate technique greatly reduces this scatter. In this technique, a second reactant with known kinetics is added to the experiment as a control, and the conversion of the control reaction is an indicator of the temperature history of the shock-heated zone. Clearly the chemical mechanism of both the test reactant and the control must not interfere with each other. The short residence time of the reaction virtually eliminates mass transfer to the walls. This is a major strength of the shock tube experiment. This strength, however, is a disadvantage if film deposition from the intermediates is desirable. In addition, the comparative rate technique is useless if no compatible control reaction is found.

Static pyrolysis is very time-consuming, laser-heated pyrolysis is expensive and may not be chemically relevant, and shock tubes have very low mass transfer rates. This paper describes an experimental system that homogeneously heats gases in the presence of heat and mass transfer. Because the effectiveness of this new reactor design is unknown, this paper describes the apparatus, its operation, and a series of experiments using reactions not associated with CVD but with known kinetic parameters. Two simple models describe the heat transfer in the reactor and its effect on the chemical dynamics. Results presented here serve two purposes:

1. They establish the range of conditions in which homogeneous reactions occur

2. They are a basis of comparison for future experiments using typical CVD precursors

Reactor Description

The principle of this reactor is quite simple: a piston in a cylinder compresses a mixture of reactant in noble gas to temperatures in excess of 1,000 K. Transport from the gas to the walls occurs continuously throughout the compression, but the cylinder walls remain at a constant temperature due to their large heat capacity (Nikanjam and Greif, 1978). In this diesel-type reactor, the low wall temperature suppresses the heterogeneous chemistry, and the compression controls the homogeneous chemistry. There are some important differences from a conventional diesel engine, however. The compression is not adiabatic—all transport phenomena are operating within the gas. The heats of reaction have much less effect on the gas temperature because the reactant is less than 1% of the mixture. In addition, the instantaneous pressure in this reactor never exceeds 250 kPa (2.5 atm).

The experimental apparatus appears in Figure 1. The reactor is a cylinder 30 cm long and has an inside diameter of 10 cm; a substrate or window closes one end of the cylinder. A piston and rod assembly slides inside the cylinder, forming a gas tight seal; a Teflon coating on the interior cylinder surface lubricates the piston seals. Heaters surround the reactor and maintain a constant surface temperature (any temperature between 25 and 200°C is possible). A pressure transducer (Teledyne-Taber model 2415, 0–345 kPa) measures the instantaneous gas pressure. The device that measures the instantaneous position of the piston is very similar to the tuning indicator of many radio receivers. In a receiver, a closed loop of nylon cord and a set of pulleys transform the rotary motion of the tuning knob into the linear motion of the indicator. In this reactor, a cord and pulley system translates the linear motion of the piston rod into the rotary motion of a 10-turn potentiometer. The potentiometer varies a voltage that is proportional to the instantaneous gas volume. A Data Translation model analog/digital converter (2801A) digitizes the output from the pressure and volume measurements and stores the data in a microcomputer. The driver gas and the mechanical trigger control the motion of the piston. Argon pressurizes the rod side of the piston to 136 kPa (5 psig), and provides the driving force for the compression. The mechanical trigger holds the piston in place until the experiment is

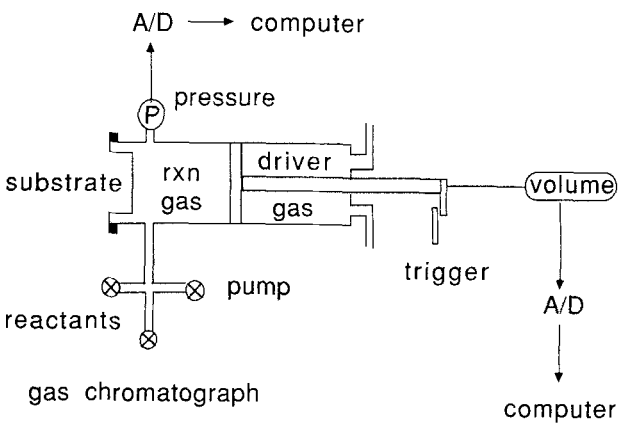

Figure 1. Prototype piston reactor.

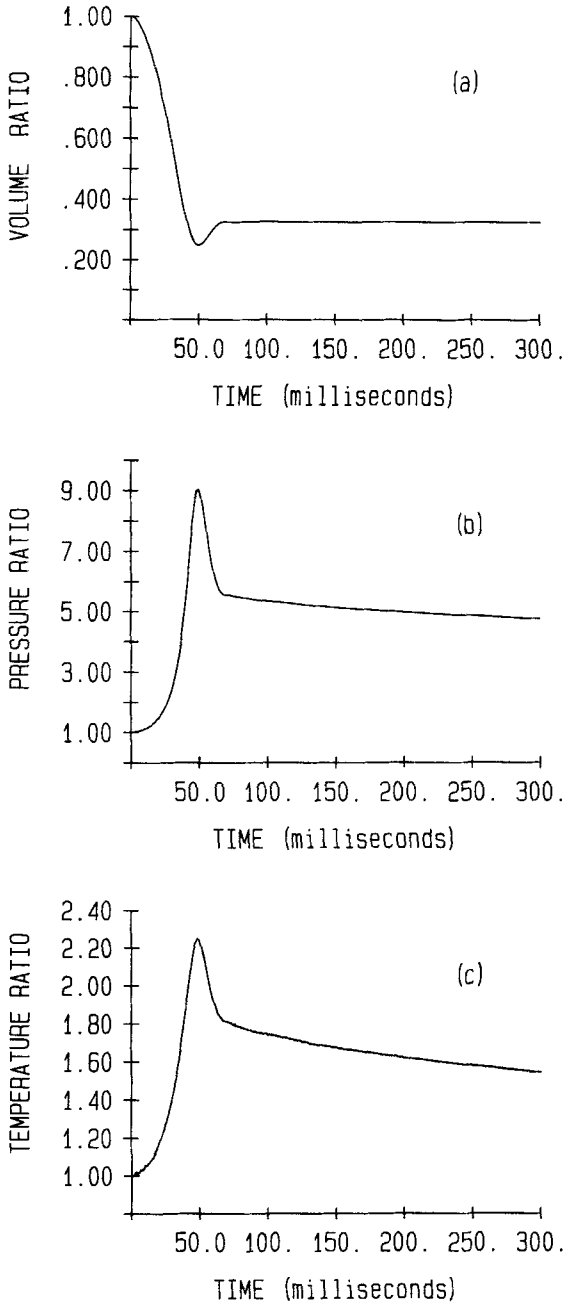

Figure 2. Volume, pressure, and mean temperature profiles of a typical compression of argon.
All profiles scaled to initial values: P_i = 26.7 kPa (200 torr); V_o = 2.6 L; T_o = 300 K
Driver pressure P_d = 136 kPa (5 psig)

ready to begin and also provides an electrical trigger for the start of data acquisition.

Operation begins with the piston fully extended and held in place by the mechanical trigger. The cylinder is evacuated and then filled with approximately 13.3 kPa (100 torr) of the gas mixture (typically, 1% reactant in argon); all valves are then closed. Pulling the mechanical trigger releases the piston and starts data acquisition. The pressurized argon forces the piston to move down the cylinder, fully compressing the reactant gases in less than 100 ms. During the initial compression, the rate of work done on the gas is greater than the instantaneous heat loss rate, and the gas rapidly heats. Unlike shock compression, the piston moves relatively slowly (<10 m/s), and there should be no large spatial distortions of the gas pressure (Nikanjam and Greif, 1978). Since the instantaneous pressure is spatially uniform and never rises above 250 kPa (2.5 atm), the ideal gas law adequately describes the mean temperature of the gas: $P(t)\,V(t) = NRT_m(t)$. As the pressure of the reactant gas rises, the piston slows to a stop, and the compression rate no longer balances the heat loss rate. At this point the gas is very hot (approximately 1,000 K), and the reactant decomposes homogeneously to form unstable intermediates. Although mass transfer occurs continuously, the wall temperature is deliberately low enough to quench heterogeneous reaction of the parent molecule. Consequently, both parent molecule and its daughters transport to the walls, but the reaction of the parent is blocked. A gas chromatograph analyzes the effluent from each experiment.

Results

Figure 2 shows the total volume, pressure, and mean temperature as functions of time for a compression of pure argon. All profiles are scaled to their initial values; for example, temperature ratio = $T_m(t)/T_m(0)$. The pressure and volume are measured values; the temperature ratio is calculated by multiplying the pressure and volume ratios. The initial conditions are given in the figure caption. The peak temperature ratio is 2.25 (675 K) and appears about 50 ms after the start of the compression. Immediately after the peak compression, the piston rebounds to a larger volume; the mass of the piston assembly and the seal friction determine the amount of rebound. Soon after the rebound, the piston stops because the friction from the seals and the reactor pressure counterbalance the driver pressure. As long as these forces sum to zero, the temperature declines in an isochoric process. At times greater than 300 ms, the falling gas temperature and pressure upset this force balance, and the piston eventually begins to close slowly. The heat transfer in this part of the profile is an isobaric process. Differentiating $V(t)$ shows that the maximum speed of the piston is <10 m/s.

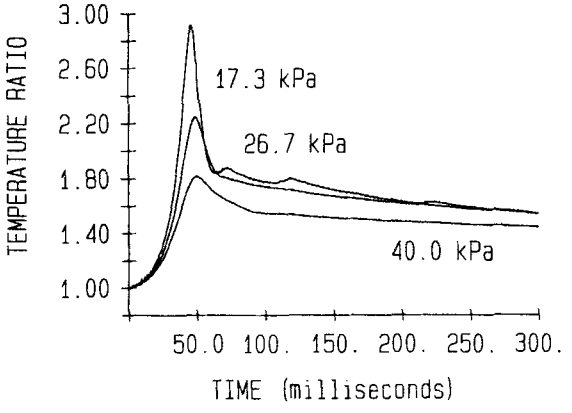

Figure 3. Temperature ratio as a function of time for various initial pressures.
Labels refer to initial pressure
P_d = 136 kPa (5 psig); T_o = 300 K

There are many factors that control the time dependence of the temperature ratio. The current configuration of the reactor uses a pneumatic driver to compress the reactants. This means the force balance on the piston controls $V(t)$ and hence $T_m(t)$. Other methods of compression would produce different profiles. The initial pressure P_i and the driver pressure P_d have a dramatic effect on the force balance and hence the temperature profile. Figure 3 shows various experiments using argon at different initial pressures. As P_i decreases, the peak temperature rises and appears at shorter times. Increasing P_d has the same effect, Figure 4. The thermal conductivity and the ratio of heat capacities, C_p/C_v, of a gas also alter $T_m(t)$. The thermal conductivity determines the heat loss rate, while the heat capacity ratio determines how the compressive work appears as gas temperature and pressure (internal energy). Gases with a low ratio have many degrees of freedom in which to store energy; therefore the temperature and pressure rise less during a compression. Figure 5 shows the results for helium, neon, argon, and nitrogen compressions. The noble gases all have the same heat capacities (on a molar basis), so only the thermal conductivity changes. As the thermal conductivity decreases with molecular weight, the temperature peak increases in height, and the temperature declines more slowly in the tail of the profile. Nitrogen, however, has a conductivity between that of neon and argon but the profile clearly shows the effect of the radically different heat capacity ratio (C_p/C_v for nitrogen is 1.40 v. 1.66 for a noble gas). Mixing in another gas also changes the effective thermal conductivity and heat capacity ratio. Figure 6 shows this result for mixtures of H_2 in argon. Generally this effect is small for less than 10% dilution. Although the initial temperature has little effect on the time dependence of the temperature ratio (except as it alters piston friction), it does scale the absolute temperature independently of all other variables. Seal integrity limits the initial temperature to less than 500 K.

The data above show that temperatures greater than 1,000 K are possible if $T_o = 500$ K. These temperatures are sufficiently high to activate most gas phase reactions. Decomposing cyclopropane, *t*-butyl alcohol, and ethyl acetate in the reactor conclusively demonstrates this fact. The reactions and their various parameters appear in Table 1. The reactions are well studied and have relatively high activation energies. The cyclopropane

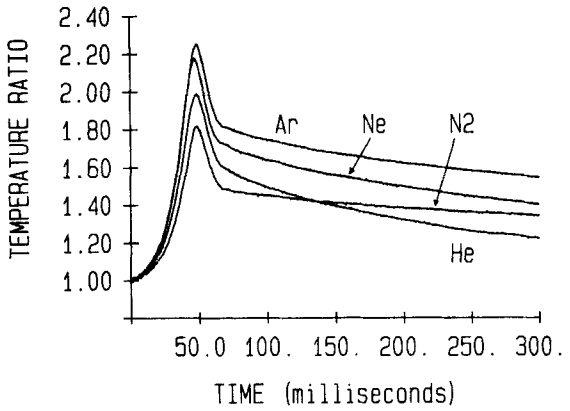

Figure 5. Temperature ratio as a function of time for various gases.
For each curve, P_i = 26.7 kPa (200 torr); T_o = 300 K; P_d = 136 kPa (5 psig)

isomerization is exothermic, while the other two reactions are endothermic. All the reactions are unimolecular decompositions and form only gaseous products; consequently, the gas chromatograph detects both products and reactant. For each reactant, the product distributions are consistent with the observations of other authors. Figure 7 shows the fraction of reactant surviving a compression as a function of peak temperature. In all cases the gas mixture is 1% reactant in argon. The data show that the fraction of the reactant remaining falls with increasing peak temperature, and that the conversions are often quite high (greater than 50%).

Discussion

Kinetics

To use the known kinetics to predict the conversions for these compressions requires numerically integrating the first-order rate equation. In general, the local rate of the irreversible reaction of $A \rightarrow B$ is

$$d[A]/dt = -k(T, P)[A] \qquad (1)$$

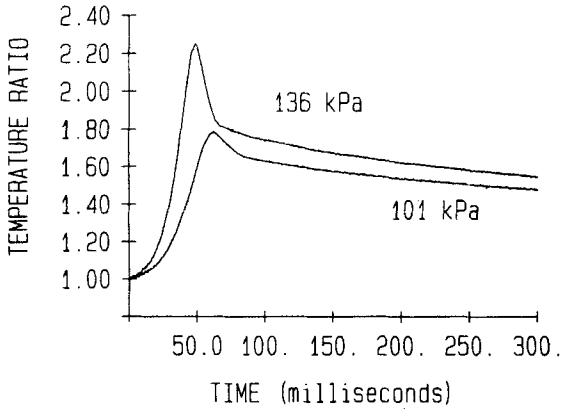

Figure 4. Temperature ratio as a function of time for two driver pressures.
Labels refer to driver pressure
P_i = 26.7 kPa (200 torr); T_o = 300 K

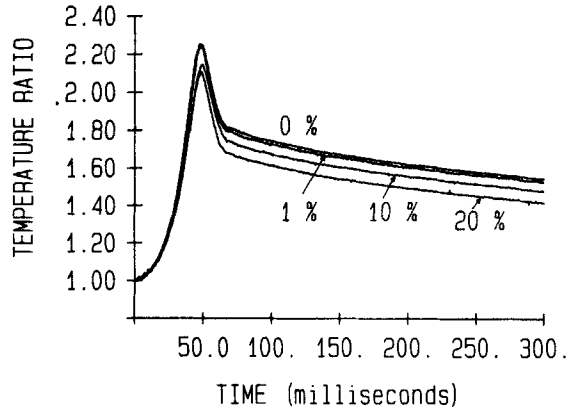

Figure 6. Temperature ratio as a function of time for various mole fractions of H_2 in argon.
Labels refer to percent H_2 in argon
P_i = 26.7 kPa (200 torr); T_o = 300 K; P_d = 136 kPa (5 psig)

Table 1. Parameters in Previous Reaction Studies

Reaction	Heat of Reaction kcal/mol	Preexp. Factor 1/s	Activation Energy kcal/mol	Temp. Range K	Ref.
Cyclopropane → propylene	−7.9	1.5×10^{15}	65.0	743–792	Chambers & Kistiakowsky (1934)
	−7.9	1.6×10^{15}	65.0	970–1265	Jeffers et al. (1973)
t-Butyl alcohol → isobutene + water	+12.8	4.8×10^{14}	65.5	778–824	Schultz & Kistiakowsky (1934)
	+12.8	4.0×10^{14}	66.2	920–1175	Lewis et al. (1974)
Ethyl acetate → acetic acid + ethylene	+14.4	3.1×10^{12}	47.8	787–883	Blades (1954)
	+14.4	4.0×10^{12}	48.0	772–1157	Beadle et al. (1972)

where $k(T, P)$ = rate constant (s^{-1}). At high enough pressures, $k(T, P)$ becomes a function of T only and assumes an Arrhenius form (Weston, 1972). In the most complicated case, $[A]$, P, and T are functions of time and position. To simplify this equation, we use the mean temperature, which is not a function of position. Assuming that the temperature is uniform and $P = P(t)$ only (the Mach number is well below 1), the ideal gas law then dictates that $[A]$ also must be uniform throughout the reactor. Consequently, integrating over the total volume at each point in time yields

$$dn/dt = -k(T, P)n \tag{2}$$

where n = the number of moles of A in the reactor. Thus the general solution for a time-varying $k(T, P)$ is

$$n/n_o = \exp\left[-\int^{t} k(T, P)\, dt'\right] \tag{3}$$

This equation is much simpler to integrate if the chemical reaction is in its high-pressure limit. Of the three test reactions, only cyclopropane remains below the high-pressure limit; the Arrhenius form is applicable for the other reactions. For cyclopropane, the conditions at the peak compression (P = 250 kPa, T = 1,000 K) are similar to the shock conditions used by Jeffers et al. (1973). For their conditions, they calculated $k(T, P)$ to be approximately 75% of the high-pressure limit. This is equivalent to a 10 K shift in temperature and is a little smaller than the expected errors of the pressure-volume measurements. Consequently, the following calculations use the Arrhenius (high-pressure) rate constant for cyclopropane also.

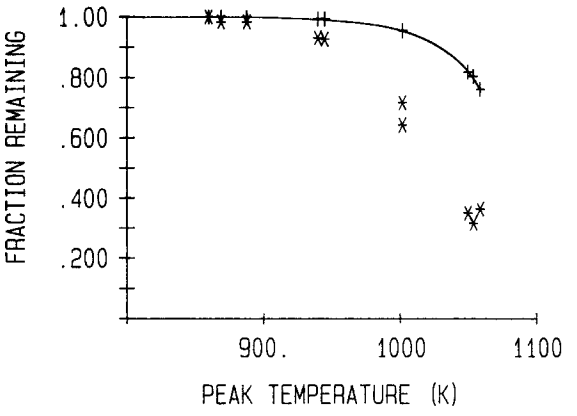

Figure 8. Fraction of cyclopropane remaining as a function of peak temperature.
*data; +calculated values

Experimental conversions from Figure 7 along with the calculated conversions appear in Figures 8 and 9 for cyclopropane and ethyl acetate, respectively. The results for *t*-butyl alcohol are not presented because inadvertent heterogeneous catalysis interfered with the results. Dohse (1929) reported that Al_2O_3 catalytically decomposes *t*-butyl alcohol at temperatures above 100°C. Unfortunately, the piston head is made of anodized aluminum and its temperature is 200°C. Consequently the results for *t*-butyl alcohol must be disregarded. The calculated conver-

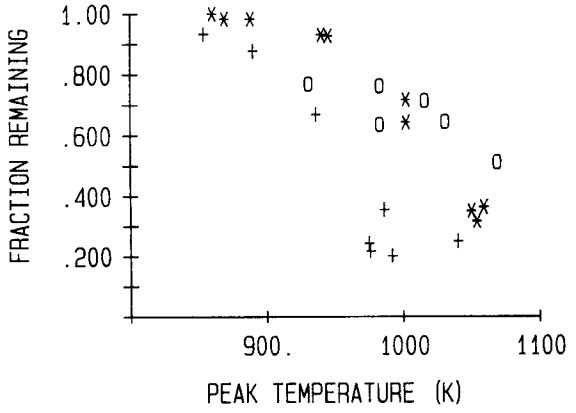

Figure 7. Fraction of reactant remaining as a function of peak temperature for three different reactions.
*cyclopropane; +ethyl acetate; O *t*-butyl alcohol

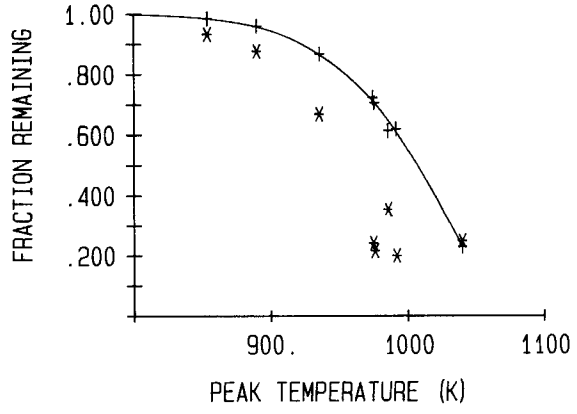

Figure 9. Fraction of ethyl acetate remaining as a function of peak temperature.
*data; +calculated values

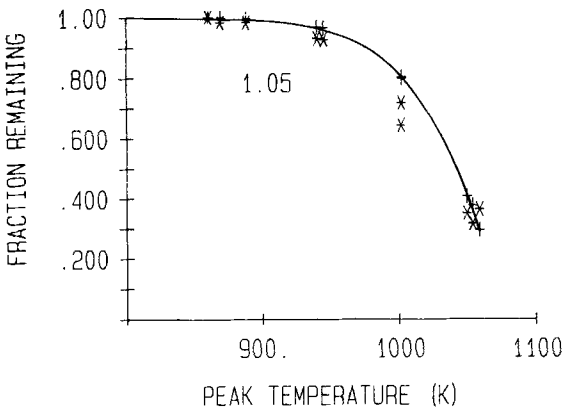

Figure 10. Fraction of cyclopropane remaining as a function of peak temperature.

*data; +prediction
Predictions calculated by multiplying the temperature profile of an experiment by correction factor 1.05 and then integrating

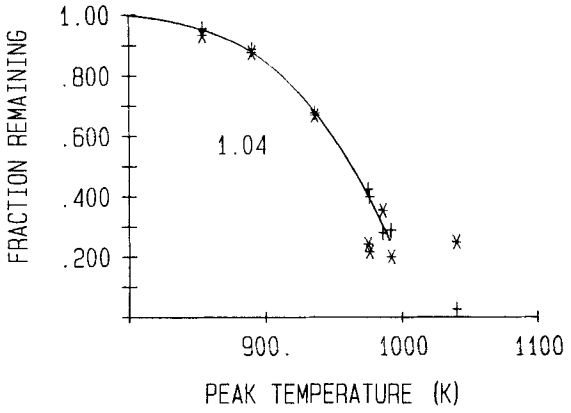

Figure 11. Fraction of ethyl acetate remaining as a function of peak temperature.

*data; +prediction
Predictions calculated by multiplying the temperature profile of an experiment by correction factor 1.04 and then integrating

sions for cyclopropane and ethyl acetate follow the trends well, but they are numerically incorrect. In every experiment, the fraction of reactant remaining is less than the calculated fraction. These disagreements are systematic.

The simplest way to bring experiment and calculation into agreement is to multiply the entire $T_m(t)$ profile of an experiment by a correction factor. This works surprisingly well. The correction factors (chosen by trial and error) for cyclopropane and ethyl acetate appear in Figures 10 and 11, respectively. The correction factor is nearly the same for both sets of data: 1.04 for ethyl acetate v. 1.05 for cyclopropane. Note that the exothermic reaction of cyclopropane has a slightly larger correction than the endothermic reaction of ethyl acetate. These corrections boost the rate constants at 1,000 K by a factor of 3 to 5. (The pressure falloff correction for cyclopropane is small compared to this.) Note that similar factors correct both sets of data even though the activation energies differ by 17 kcal/mol. Furthermore, the correction factor improves the fit at each data point—all the calculated points need about the same correction. These facts indicate a systematic error. Keep in mind, however, that this correction is relatively small (<5%).

The systematic error lies with either the pressure-volume measurement or a faulty assumption in the kinetic calculation. Since the largest fraction of chemical reaction occurs at the highest temperatures, a subtle error in the pressure-volume measurements appears as a grave distortion in the calculated conversion. First consider the pressure measurement. It is susceptible to distortion as pressure changes move through the tube connecting the pressure sensor to the reactor. Van Aken (1977) has studied such pressure distortions in combustion engines, and he reports two effects: (1) an overshoot in the peak pressure (which would not explain the errors in the piston reactor), and (2) a time lag in the appearance of the pressure peak (which could explain the errors). Both these distortions increase with increasing tube length. Increasing the tube length in the reactor has no detectable effect on the height or shape of $P(t)$. Ideally, a transducer mounted flush in the hot reactor wall would remove this uncertainty completely. Another possible source of error lies in the volume measurement. The high rates of compression may generate small hystereses in the volume measurements (e.g., cord stretch). These hystereses (which are undetectable at the initial volume) become proportionally larger at the final volume and may systematically alter the maximum temperature. Only more sophisticated equipment can resolve this problem.

The more likely cause of the discrepancy is the use of the mean temperature in the Arrhenius calculation. Figure 12 shows a typical temperature profile at a particular point in time as a function of distance from the reactor wall, x. Also included is the concentration profile as deduced from the ideal gas law, $P = cRT$. For a given mass and pressure, we can calculate the mean concentration and from that, the mean temperature. In the real temperature profile, the exponential character of the rate constant causes the maximum temperature plateau to dominate the overall reaction rate. Although the mean temperature may be only slightly smaller than the maximum temperature, conversions calculated using it would be significantly too low. If the temperature gradients in the boundary region are steeper, the difference between the mean and maximum is less. Hence the pressure-volume procedure "sees" the mean temperature, and the kinetics "see" the maximum temperature. Since the correction factor is about 5% in every case, this indicates that the maximum temperature is about 5% higher than the mean temperature and that the heat transfer characteristics of argon largely control the correction.

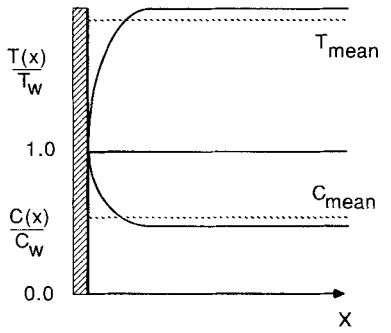

Figure 12. Typical temperature profile and related concentration profile as functions of distance from reactor wall.

Heat transfer

Not surprisingly, the heat transfer indirectly governs the kinetics. Studying the heat transfer gives some insight into the physics of the reactor and the effect on the kinetics. The first step is to determine the flow fields present in a piston compression. The internal combustion literature contains many studies of flows in piston compressions. There are only a few studies, however, where combustion dynamics or turbulence induced by valves do not dominate the flows. Tabaczynski et al. (1970) and Daneshyar et al. (1973) show that a vortex forms at the interface between the piston face and the stationary wall. Bernard (1981) has reproduced these experimental results in a two-dimensional numerical simulation. These works show that the area of the vortex divided by the square of the stroke is a function of the mean Reynolds number. The vortices are usually small but become a larger fraction of the total volume as the compression volume decreases. Results for heat transfer in a piston compression (with no reaction) are limited. Greif and coworkers (Nikanjam and Greif, 1978; Greif et al., 1979) have measured and modeled the unsteady heat transfer rates found in the initial stages of a fast piston compression. Their conditions are very similar to the conditions in this work. Their calculations show that the bulk of the gas compresses isentropically; temperature gradients exist only in a thin boundary layer. At the highest compression ratios, the calculations of the heat transfer in the boundary layer fall short of the experimental results. They attribute this to the vortex enhancing heat transfer.

In the current system the pressure-volume data indicate three distinct regions, Figure 2. During the first 25 ms of the experiment, the compression proceeds isentropically and the pressure-volume data follow the well known PV^{γ} relationship. This region is consistent with the results of Greif and coworkers. The isentropic compression breaks down during the next 40–50 ms, presumably because of the rising temperature which increases heat conduction and because of the growth of the vortex turbulence. The turbulence should continue to grow as long as the piston closes; during the piston rebound, the effect on the overall turbulence level is unknown. For times greater than 75 ms (stationary piston), conduction continues, the vortices decay, and free convection (if any) begins to develop.

Describing completely the transport phenomena found near the peak temperature is very difficult. Clearly, unsteady conduction and vortex flows both determine the spatial temperature distribution at this point in time. Previous work has shown that vortices are local phenomena. We propose to make some extreme assumptions to simplify the physics and use only the unsteady conduction to describe the isochoric cooling of the gas. Any vortices present should have a large impact on the isochoric cooling since there is no compressive heating. Thus, neglecting vortices is a sensitive test of their relative importance. Despite the severity of the assumptions, the results are surprisingly consistent with experimental data.

Assuming that the gas is stationary, the differential equation describing the temperature in the gas is (Bird et al., 1960)

$$\rho \hat{C}_v \frac{\partial T}{\partial t} = cC_v \frac{\partial T}{\partial t} = -\nabla \cdot (-k \nabla T) \tag{4}$$

where ρ = gas density, $\hat{C}_v$ = constant volume heat capacity (J/g · K), c = molar concentration, C_v = constant volume heat capacity (J/mol · K), and k is the thermal conductivity. The temperature of the gas at all boundaries is equal to the wall temperature. This equation is much simpler to solve if k is constant relative to the spatial derivative. For monatomic gases at pressures less than a few atmospheres, the thermal conductivity is roughly proportional to the square root of the absolute temperature and independent of pressure. If the gas temperature at the center of the piston is 1.5 times the wall temperature, then k at the center of the piston is only about 1.2 times the thermal conductivity at the wall. Therefore as a first approximation, we assume that k is a constant in all the spatial derivatives and group the ratio k/cC_v into D_v, the thermal diffusivity (constant volume). Using $c = P/RT$ and a Chapman-Enskog representation for k (Reid et al., 1977), D_v can be calculated at any point in time. The thermal diffusivity does not vary substantially over time because the temperature falls less than 100 K before the piston begins its slow compression and the reactor geometry varies in time. Since $D_v \approx$ constant, the solutions to Eq. 4 are analytical.

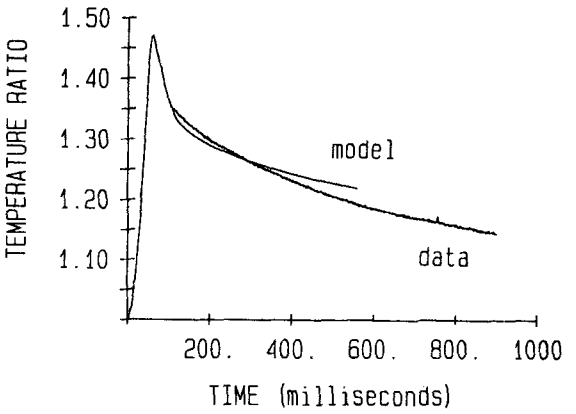

Figure 13. Experimental temperature profile and predicted results using unsteady conduction model.
$D_v = 1.22$ cm^2/s; $l = 8.2$ cm; $T_i/T_w = 1.36$

Assuming that the initial condition is not a function of position, $T(z, r, t = 0) = T_i$, where z = axial length from the midpoint, r = radial distance, and t = time. For a finite cylinder with constant wall temperature, Carslaw and Jaeger (1980) give the solution to Eq. 4 as

$$\frac{T(r,z,t) - T_w}{T_i - T_w} = \sum_{n=0}^{\infty} \sum_{m=1}^{\infty} \left\{ \frac{4(-1)^n}{\pi(2n+1)} \cos\left[\frac{(2n+1)\pi z}{2l}\right] \right\} \cdot \left[\frac{2J_0(r\alpha_m)}{a\alpha_m J_1(a\alpha_m)}\right] \cdot \exp\left\{-D_v t\left[\alpha_m^2 + \frac{(2n+1)^2\pi^2}{4l^2}\right]\right\} \tag{5}$$

where T_w = wall temperature
a = radius of the cylinder = 5 cm
l = half the axial length
J_i = Bessel functions of ith order
α_m = roots of the equation $J_0(\alpha_m a) = 0$.

By evaluating the temperature gradients at the walls, calculation of the amount of heat loss is possible. From this, we calculate the fraction of heat remaining in the gas as a function of

time; this quantity is directly proportional to $T_m - T_w$:

$$\frac{T_m(t) - T_w}{T_i - T_w} = 32\left\{\sum_{n=0}^{\infty} \exp\left[\frac{-D_v\pi^2(2n+1)^2t}{4l^2}\right]\right\} \cdot \left[\sum_{m=1}^{\infty} \frac{\exp(-D_v\alpha_m^2 t)}{(a\alpha_m)^2}\right] \quad (6)$$

This equation predicts *a priori* the time dependence of T_m. Figure 13 shows an example of the fit for an experiment using argon. The volume is constant only in the region spanned by the model curve. The fit is remarkable considering the model uses no adjustable parameters and ignores vortex convection. This model fits other data from experiments using helium, neon, and argon at two different wall temperatures.

The model predicts heat transfer rates that are too high at short times; if vortex flow dominated, the unsteady conduction calculation should have underpredicted the rate. Apparently the completely uniform temperature at time = 0 actually overcompensates for omitting the local vortices. However, substituting a well-developed temperature distribution into Eq. 4 grossly underpredicts the heat transfer. Thus, using steep (but not infinite) temperature gradients at the walls for time = 0 is sufficient to explain the data; vortices are probably a small contribution to heat transfer. At longer times, the unsteady conduction equation predicts a lower heat transfer rate than the data show. Heat transfer due to vortices cannot explain this result because vortices should decay with time and therefore have less impact as time increases. Possibly free convection begins to develop on this time scale.

Dimensional analysis can test whether free convection is an important form of heat transfer at longer times. Assuming no compressive work, a total energy balance on the gas requires

$$NC_v dT_m/dt = hA(T_w - T_m) \quad (7)$$

where h = heat transfer coefficient, and A = heat transfer area of the finite cylinder. In terms of dimensionless variables,

$$d[\tau - 1]/dt = (NukA)/(DNC_v)[1 - \tau] \quad (8)$$

where $\tau = T_m/T_w$, Nu = Nusselt number = hD/k, D = diameter of the cylinder (10 cm), and k = thermal conductivity of the gas. Assuming that Nu and k are constant, a plot of ln $[\tau - 1]$ vs. t yields a straight line with a slope proportional to Nu. Indeed, such plots of the experimental data are nearly straight lines and determine the value of Nu for that experiment.

Dimensional analysis for a simple cylindrical geometry predicts that Nu has the following functional dependence (ignoring vortex flow):

$$Nu = f(Pr, L/D, Gr) \quad (9)$$

where Pr = Prandtl number, L = cylinder length during cooling, and Gr = Grashof number. For noble gases $Pr = \frac{2}{3}$ for all experiments, L/D is a constant during an individual experiment, and Gr does not vary greatly during the isochoric heat transfer. Consequently the assumption Nu = constant is a good one, and Nu should correlate with L/D and Gr only. Typically the correlation

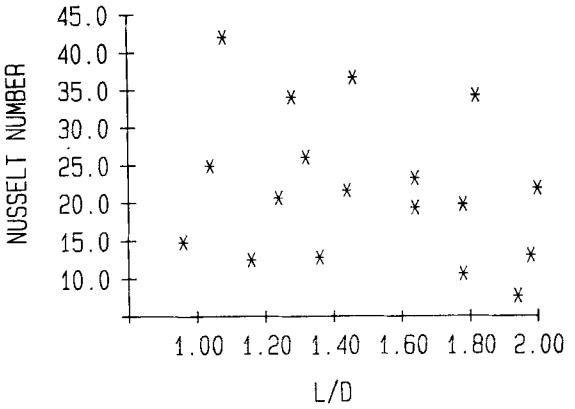

Figure 14. Nusselt number as a function of L/D for a variety of experiments.
Gases included helium, neon, argon; no correlation seems to exist

has the form

$$Nu = \text{constant}\ (L/D)^i Gr^j \quad (10)$$

Ignoring the Gr dependence of the correlation, Figure 14 shows the relationship between Nu and L/D. No correlation is obvious. Including the Gr dependence, a multivariable linear regression of Eq. 10 indicates $i = -0.25$ and $j = 0.25$. The correlation appears in Figure 15 along with a best fit line. The data come from experiments using argon, neon, and helium at a variety of initial conditions. Clearly some convective flow is important at longer times.

These analyses of heat transfer have interesting implications for the chemical dynamics of the reactor. The unsteady conduction results imply that the boundary layers control most of the transport processes at short times, but the Grashof correlation shows that convective flows will dominate the transport if given enough time. Consequently, during a fast compression, the reactive intermediates are confined to a central core region where the temperature is the highest (about 5% higher than the mean temperature). As the compression slows (in the above analysis, the compression rate is zero), bulk flow begins to dominate. Heat and the reactive intermediates transport to the walls, and cold gas near the walls moves into the central core.

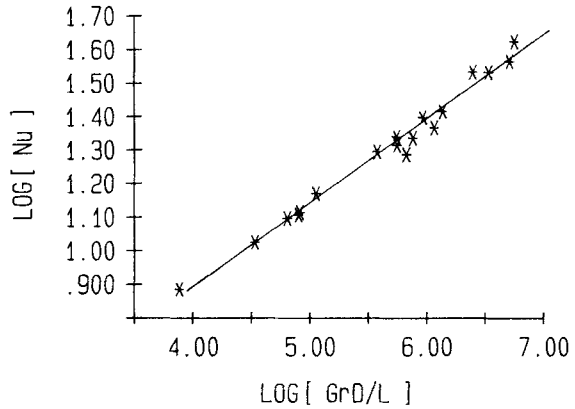

Figure 15. Log Nu as a function of log $[Gr(L/D)^{-1}]$.
Slope of best fit line is 0.250

Conclusions

The piston reactor can compress reactant gases to the high temperatures found in chemical vapor deposition (>1,000 K) using a simple and inexpensive apparatus. Pressure and volume measurements record the mean temperature of the gas. Test reactions show that large conversions are possible over a broad range of conditions. Comparison of experimental conversions with conversions calculated from $T_m(t)$ show that the maximum temperature is approximately 5% above the mean temperature, and a simple analytical method can correct these errors. Two models describe the isochoric heat transfer from the gas. At long times, dimensional analysis correlates the heat transfer coefficient with geometry (L/D) and free convection (Gr). At short times, the unsteady conduction equation reproduces the time dependence of the temperature using no adjustable parameters. These results indicate that conduction dominates heat transfer during short time scales, but macroscopic heat transfer (convection) dominates at longer times.

This reactor has some very powerful advantages to be exploited. Since the heating method is simple compression, the results are directly comparable to shock tube experiments but with subtle differences. Unlike shock experiments, the reactor does not need *in situ* comparative rate techniques; the correction factor and $T_m(t)$ provide the necessary calibration. Thus the reactor completely avoids the possible interaction of the control reaction and the test reaction. The large reaction volume and relatively long reaction times (which the investigator could control using a different compression method) should simplify the optical detection of reactive intermediates currently observed in shock tubes. Its most important advantage, however, is the independent control of the heterogeneous and homogeneous chemistries in the presence of transport phenomena. Low substrate temperature quenches the heterogeneous chemistry of the precursor, and the compression activates the homogeneous chemistry.

Acknowledgment

Grants from IBM, Xerox, the National Science Foundation, Grant No. MSM84-51234, the Universitywide Energy Research Group, and the Chancellor's Patent Fund have supported this work. The authors gratefully acknowledge equipment, facilities, and advice supplied by James Michaels and David Graves.

Notation

a = radius of cylinder = 5 cm
A = surface area of piston, cm^2
$[A]$ = molar concentration of reactant A
c = molar gas concentration, mol/cm^3
C_p = molar heat capacity (constant pressure), J/mol · K
$\hat{C}_p$ = molar heat capacity (constant pressure), J/g · K
C_v = molar heat capacity (constant volume), J/mol · K
$\hat{C}_v$ = heat capacity (constant volume), J/g · K
D = cylinder diameter = 10 cm
D_v = thermal diffusivity, cm^2/s
g = gravitational constant = 980 cm/s^2
Gr = Grashof number = $gD^3\rho^2(T_m - T_w)/(T_m\mu^2)$
h = heat transfer coefficient, W/m^2 · K
i = constant in Nusselt number correlation
j = constant in Nusselt number correlation
J_i = Bessel function of ith order
k = thermal conductivity, W/m · K
$k(T, P)$ = unimolecular rate constant, s^{-1}
l = half the axial length, cm
L = length of cylinder during constant volume heat loss
$n(t)$ = number of moles of reactant
n_o = initial number of moles of reactant
N = total number of moles of gas in reactor
Nu = Nusselt number = hD/k
P = pressure, kPa
P_d = driver pressure, kPa
P_i = initial pressure, kPa
Pr = Prandtl number = $\hat{C}_p\mu/k$ = 2/3 for noble gases
R = ideal gas constant
T = temperature, K
T_i = initial temperature for modeling, K
T_o = initial temperature, K
T_m = mean temperature, K
T_w = wall temperature, K
t = time, s
$V(t)$ = total volume, cm^3
V_o = initial volume, L
x = spatial dimension
y = spatial dimension
z = spatial dimension

Greek letters

α_m = roots of the equation $J_o(\alpha_m a) = 0$
μ = viscosity, g/cm · s
ρ = gas density, g/cm^3
τ = ratio of T_m and T_w

Literature Cited

Beadle, P. C., D. M. Golden, and S. W. Benson, "Very Low Pressure Pyrolysis. IV: The Decomposition of Ethyl Acetate," *Int. J. Chem. Kinetics*, **4**, 265 (1972).

Bernard, P. S., "Computation of the Turbulent Flow in an Internal Combustion Engine During Compression," *J. Fluids Eng.*, **103**, 75 (1981).

Bilenchi, R., M. Musci, and R. Murri, "Large-Area Deposition of Hydrogenated Amorphous Silicon by CW CO_2 Lasers," SPIE *Laser-Assisted Deposition, Etching, Doping*, **459**, 61 (1984).

Bird, R. B., W. E. Stewart, and E. N. Lightfoot, *Transport Phenomena*, Wiley, New York, 322 (1960).

Blades, A. T., "The Kinetics of the Pyrolysis of Ethyl and Isopropyl Formates and Acetates," *Canad. J. Chem.*, **32**, 366 (1954).

Carslaw, H. S., and J. C. Jaeger, *Conduction of Heat in Solids*, Clarendon, Oxford, 1980.

Chambers, T. C., and G. B. Kistiakowsky, "Kinetics of the Thermal Isomerization of Cyclopropane," *J. Am. Chem. Soc.*, **56**, 399 (1934).

Daneshyar, H., D. E. Fuller, and B. E. L. Deckker, "Vortex Motion Induced by the Piston of an Internal Combustion Engine," *Int. J. Mech. Sci.*, **15**, 381 (1973).

Deutsch, T. F., "Infrared Laser Photochemistry of Silane," *J. Chem. Physics*, **70**, 1187 (1979).

Dohse, H., "Zur Kenntnis heterogener Spaltungsreaktionen. II," *Z. physik. Chem.*, **B6**, 343 (1929).

Flint, J. H., M. Meunier, D. Adler, and J. S. Haggerty, "A-Si:H Films Produced from Laser-Heated Gases: Process Characteristics and Film Properties," SPIE *Laser-Assisted Deposition, Etching, Doping*, **459**, 66 (1984).

Greif, R., T. Namba, and M. Nikanham, "Heat Transfer During Piston Compression Including Side Wall and Convection Effects," *Int. J. Heat Mass Trans.*, **22**, 901 (1979).

Jeffers, P., D. Lewis, and M. Sarr, "Cyclopropane Structural Isomerization in Shock Waves," *J. Phys. Chem.*, **77**, 3037 (1973).

Lewis, D., M. Keil, and M. Sarr, "Gas Phase Thermal Decomposition of tert-Butyl Alcohol," *J. Am. Chem. Soc.*, **96**, 4398 (1974).

Newman, C. G., H. E. O'Neal, M. A. Ring, F. Leska, and N. Shipley, "Kinetics and Mechanism of the Silane Decomposition," *Int. J. Chem. Kinetics*, **11**, 1167 (1979).

Nikanjam, M., and R. Greif, "Heat Transfer During Piston Compression," *J. Heat Trans.*, **100**, 527 (1978).

Purnell, J. H., and R. Walsh, "The Pyrolysis of Monosilane," *Proc. Roy. Soc. A*, **293**, 543 (1966).

Reid, R. C., J. M. Prausnitz, and T. K. Sherwood, *The Properties of Gases and Liquids*, McGraw-Hill, New York (1977).

Schultz, R. F., and G. B. Kistiakowsky, "The Thermal Decomposition of

Tertiary Butyl and Tertiary Amyl Alcohols. Homogeneous Unimolecular Reactions," *J. Am. Chem. Soc.*, **56**, 395 (1934).
Tabaczynski, R. J., D. P. Hoult, and J. C. Keck, "High Reynolds Number Flow in a Moving Corner," *J. Fluid Mech.*, **42**, 249 (1970).
Van Aken, I. C., "Adapter Errors in Indicator Diagrams of Combustion Engines," *Proc. Inst. Mech. Eng.*, **191**, 125 (1977).
Weston, R. E., Jr., and H. A. Schwarz, *Chemical Kinetics*, Prentice-Hall, Englewood Cliffs, NJ (1972).
White, R. T., R. L. Espino-Rios, D. S. Rogers, M. A. Ring, and H. E. O'Neal, "Mechanism of the Silane Decomposition. I: Silane Loss Kinetics and Rate Inhibition by Hydrogen. II: Modeling of the Silane Decomposition (All Stages of Reaction)," *Int. J. Chem. Kinetics*, **17**, 1029 (1985).

Manuscript received Mar. 2, 1987, and revision received June 19, 1987.